01 Jan 2016

Strain Distribution and Crack Detection in Thin Unbonded Concrete Pavement Overlays with Fully Distributed Fiber Optic Sensors

Yi Bao

Genda Chen
Missouri University of Science and Technology, gchen@mst.edu

Recommended Citation

Y. Bao and G. Chen, "Strain Distribution and Crack Detection in Thin Unbonded Concrete Pavement Overlays with Fully Distributed Fiber Optic Sensors," *Optical Engineering*, vol. 55, no. 1, SPIE, Jan 2016. The definitive version is available at https://doi.org/10.1117/1.OE.55.1.011008

Optical Engineering

OpticalEngineering.SPIEDigitalLibrary.org

Strain distribution and crack detection in thin unbonded concrete pavement overlays with fully distributed fiber optic sensors

Yi Bao
Genda Chen

SPIE.

Strain distribution and crack detection in thin unbonded concrete pavement overlays with fully distributed fiber optic sensors

Yi Bao and Genda Chen*
Missouri University of Science and Technology, Department of Civil, Architectural, and Environmental Engineering, 1401 North Pine Street, Rolla, Missouri 65409-0030, United States

Abstract. This study aims at evaluating the feasibility of strain measurement and crack detection in thin unbonded concrete pavement overlays with pulse prepump Brillouin optical time domain analysis. Single-mode optical fibers with two-layer and three-layer coatings, respectively, were applied as fully distributed sensors, their performances were compared with analytical predictions. They were successfully protected from damage during concrete casting of three full-scale concrete panels when 5 to 10-cm-thick protective mortar covers had been set for 2 h. Experimental results from three-point loading tests of the panels indicated that the strain distributions measured from the two types of sensors were in good agreement, and cracks can be detected at sharp peaks of the measured strain distributions. The two-layer and three-layer coated fibers can be used to measure strains up to 2.33% and 2.42% with a corresponding sensitivity of 5.43×10^{-5} and 4.66×10^{-5} GHz/$\mu\varepsilon$, respectively. Two cracks as close as 7 to 9 cm can be clearly detected. The measured strains in optical fiber were lower than the analytical prediction by 10% to 25%. Their difference likely resulted from strain transfer through various coatings, idealized point loading, varying optical fiber embedment, and concrete heterogeneity. [DOI: 10.1117/1.OE.55.1.011008]

Keywords: strain distribution; crack detection; concrete pavement; fully distributed fiber optic sensor; pulse prepump Brillouin optical time domain analysis.

Paper 150633SS received May 14, 2015; accepted for publication Sep. 23, 2015; published online Oct. 20, 2015.

1 Introduction

The amount of paved public roads and streets in the U. S. exceeded 2.65 million miles in 2012. With increasing traffic volume and vehicle weight as a result of urbanization many of the existing roads and streets have deteriorated at an accelerated pace and must be rehabilitated. Among various rehabilitation methods, unbonded pavement overlaying has recently received increasing attention due to its cost-effectiveness, durability, and recyclability.[1–3] It does not require any surface preparation of existing pavement and is not susceptible to potential cracking in the existing pavement. For example, thin concrete panels reinforced with alloy polymer macrosynthetic fibers have been introduced to rapidly and cost-effectively improve the driving conditions of existing roadways by first laying down a fabric sheet on the roadways, then casting a thin layer of concrete, and finally cutting the layer into the required panels. These panels are vulnerable to cracking due to reduced thickness. Therefore, it is imperative to monitor strains and potential cracks in thin concrete panels.

Various monitoring technologies have been developed to measure strain and detect cracking in concrete.[4–12] For example, vibrating wire and fiber Bragg grating sensors were deployed for strain measurement[4–6] and the detection of cracks when they happen to pass across the sensors. In most cases, however, it is difficult to accurately predict crack locations in pavement before sensors are placed. Although a large number of sensors can be blindly deployed over a large area for crack detection, they may be cost prohibitive and could potentially influence the behavior of the structures. In particular, for thin pavement overlays, the presence of sensors may significantly influence the strain distribution in pavement, depending on their size relative to the overlay thickness. An acoustic emission technique[7] was also applied to detect cracking. It does not provide strain measurements. More importantly, the success interpretation of recorded data largely depends on the use of a signal filter since the measured signals are usually very noisy. Coaxial cables[8] were also introduced to detect cracking in full-scale columns, girders, and bridges. However, they are commercially unavailable at the present time.

On the other hand, fully distributed fiber optic sensors have attracted intensive research interest worldwide due to their many advantages such as long-range continuous measurement, cost-effectiveness, immunity to electromagnetic interference, and resistance to harsh environments.[9,10] In particular, Brillouin scattering provides an excellent opportunity for distributed sensing of both strain and temperature along an optical fiber. The so-called spontaneous scattering is used in Brillouin optical time domain reflectometry (BOTDR) measured from one end of the fiber, and the stimulated scattering in Brillouin optical time domain analysis (BOTDA) measured from two ends of the fiber loop.[11] In these applications, a telecom grade single-mode fiber (SMF) functions as a distributed sensor and a transmission cable. BOTDA was applied to detect cracks in steel girders.[12] BOTDR was used to monitor the stress of post-tensioning

*Address all correspondence to: Genda Chen, E-mail: gchen@mst.edu

0091-3286/2015/$25.00 © 2015 SPIE

cable in a concrete reinforced beam,[13] and the structural defects in a steel beam.[14] However, the spatial resolution of BOTDA and BOTDR is in the order of 0.5 to 1.0 m,[10,11,15] which makes it challenging to monitor microcracks in various infrastructures. A special design and installation of a distributed fiber optic sensor was applied to manipulate delamination between the optical fiber and the monitored host structure.[16] The delamination resulted in an extra length to average the crack-induced length change in the optical fiber, which enables submillimeter cracks to be detected using BOTDA.[16] Rayleigh scattering has also been implemented for distributed strain measurements with improved spatial resolution.[15] However, compared with stimulated Brillouin scattering technologies (e.g., BOTDA), Rayleigh scattering and spontaneous Brillouin scattering-based technologies are limited in their maximum sensing length.[15] Recently, pulse prepump Brillouin optical time domain analysis (PPP-BOTDA) has been proposed to take advantage of a prepump pulse that further stimulates the phonon before a narrow bandwidth pulse arrives, thus a centimeter spatial resolution was achieved.[17]

In this study, PPP-BOTDA is for the first time proposed to monitor strain distribution and crack detection in thin unbonded concrete pavement panels. Three full-scale (183 cm × 183 cm × 7.5 cm) panels were fabricated and instrumented with two types of single mode optical fibers as distributed sensors. The mechanical properties of optical fibers were experimentally determined and their strain sensitivity coefficients were calibrated using a low capacity load frame. Considering the fragile nature of fiber sensors, an installation method was developed and implemented during the casting of full-scale concrete panels. Each panel was loaded to failure with three-point bending tests. The strain measured from PPP-BOTDA was compared with the analytical prediction to understand the potential effect of strain transfer through one or more coating layer(s) of an optical fiber. Multiple cracks were identified from the measured strain distributions, from which the spatial resolution of closely spaced cracks was examined.

2 Sensing Principle of Pulse Prepump Brillouin Optical Time Domain Analysis

Brillouin scattering in an optical fiber describes the interaction of an incident light wave with an acoustic wave associated with the variation of characteristic density along the fiber. As shown in Fig. 1, PPP-BOTDA measures strain and temperature variations by sending a pump pulse wave and a probe continuous wave counter-propagating from two ends of an optical fiber, resulting in stimulated Brillouin scattering.[17] When the frequency difference between the pulse and continuous waves matches with the Brillouin frequency of the optical fiber, Brillouin gain or loss occurs and changes with the density of the fiber medium.

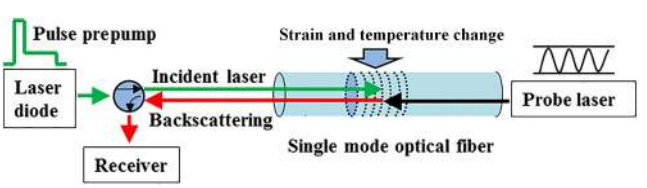

Fig. 1 A typical pulse pre-pump Brillouin optical time domain analysis (PPP-BOTDA) system.

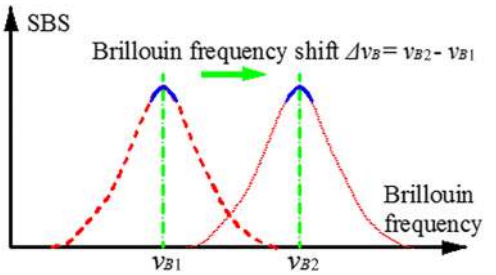

Fig. 2 Sensing principle of PPP-BOTDA.

Compared with conventional BOTDA, PPP-BOTDA takes advantage of a PPP that stimulates the phonon before its following narrow bandwidth pulse arrives, greatly improving the spatial resolution. With a pulse bandwidth of 0.2 ns, a 2-cm spatial resolution is obtainable over a 0.5 km measurement distance, and 15 $\mu\varepsilon$ and 0.75°C measurement accuracies can be respectively achieved for strain and temperature with an average count of 2.[15] The backward Brillouin scattering frequency ν_B is on the order of 9 to 13 GHz for light waves of 1.3 to 1.6 μm wavelengths in a standard SMF. This is given by Eq. (1):[10]

$$\nu_B = 2nV_a/\lambda, \tag{1}$$

where n is the effective refractive index; V_a is the acoustic velocity; and λ represents the wavelength of the laser source.

The shift in Brillouin frequency $\Delta\nu_B$ as illustrated in Fig. 2 can be related to the strain and temperature changes in an optical fiber.[11] That is,

$$\Delta\nu_B = C_\varepsilon\Delta\varepsilon + C_T\Delta T, \tag{2}$$

where C_ε and C_T denote the strain and the temperature coefficients, respectively; $\Delta\varepsilon$ and ΔT denote the strain and the temperature changes, respectively.

3 Characterizations of Optical Fibers

In this study, two types of telecom grade SMFs were used as distributed fiber optic sensors based on the PPP-BOTDA. As shown in Fig. 3, they are SMFs packaged with two layers of polymer coating (2C fiber) and a three-layer coating (3C fiber), respectively. Each SMF is composed of an 8.2-μm-diameter glass core and a 125-μm-diameter glass cladding. The outer diameters of 2C and 3C fibers are 242 and 880 μm, respectively. The inner coating (190 μm in outer diameter) is soft and can protect the glass from mechanical impact. The outer coating is stiff and can protect the glass from abrasion and environmental exposure. To further enhance its mechanical strength, the 3C fiber is packaged with an additional layer of tight buffer. Each of the three layers (the inner and outer coatings as well as the tight buffer) is composed of complex mixtures of raw materials such as monomers, oligomers, photoinitiators, and additives.

The ultimate load and maximum strain of optical fibers were experimentally determined from uniaxial tensile tests on a low capacity load frame with a load cell of 100 N at room temperature (22°C). The tests were conducted under displacement control at a loading rate of 1 mm/min. The applied load and extension were simultaneously measured

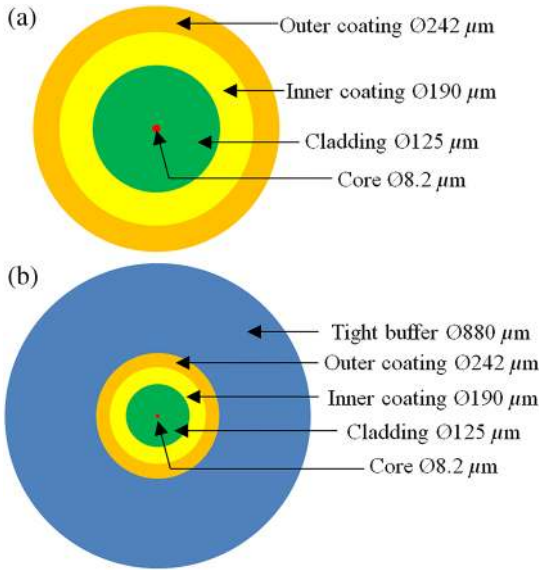

Fig. 3 Cross sections: (a) 2C fiber and (b) 3C fiber.

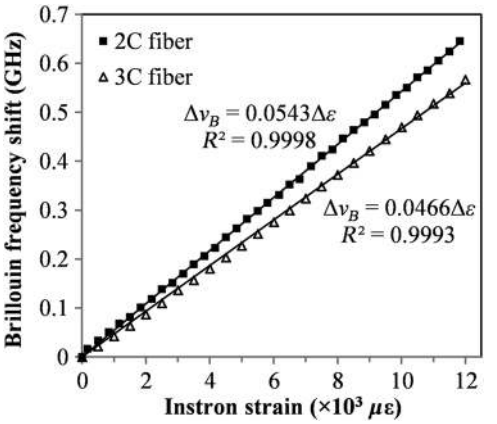

Fig. 4 Calibration of the distributed sensor with PPP-BOTDA.

and recorded by internal transducer and extensometer, respectively. Given the initial length of each fiber, the strain in the fiber can be evaluated and the load-strain relation can be determined. Considering the fragile nature of the fiber, the gripping area at each end of the fiber was strengthened by a protective sleeve, which is typically used to protect fusion splices. Each sleeve has a steel bar inside, and thus can be directly gripped by the load frame.

During the tensile tests, both types of optical fibers fractured in a brittle manner. The applied load increased linearly with strain until failure. Ten 2C fibers and 10 3C fibers were tested. For the 2C fibers, the average values of the 10 ultimate loads and the 10 maximum strains were 22.6 N and 23.3×10^3 $\mu\varepsilon$, respectively. The maximum strain determines the sensor's operation range for strain measurement. For the 3C fibers, the average values of the 10 ultimate loads and the 10 maximum strains were 25.2 N and 24.2×10^3 $\mu\varepsilon$, respectively. Although the increase in ultimate load and maximum strain when using the additional tight buffer in the 3C fibers was small, the shear strength of the 3C fibers has been shown to be approximately four times that of the 2C fibers[18] because of the enlarged cross sections. The increased shear strength of the 3C fibers can ensure their survivability during installation, concrete casting, and long-term operation.

Another test was performed at room temperature to calibrate the strain sensitivity coefficient of the sensors. Each type of optical fiber was tension loaded with an incrementally increasing load. At each load, the Brillouin frequency shift of the optical fiber due to strain change was measured from a Neubrescope (Neubrex NBX-7020). The measured Brillouin frequency shift can be linearly correlated with the evaluated strain from the directly measured extension on the load frame, as indicated in Eq. (2). Figure 4 shows the measured Brillouin frequency shift from each optical fiber as a linear function of the applied strain obtained from the load frame. The coefficient of determination (R^2 factor) for the linear regression is close to 1.0, indicating a good correlation. The slope of each line represents the frequency-strain coefficient of the optical fiber sensor. Therefore, the strain sensitivity coefficients of 2C and 3C optical fibers are approximately 5.43×10^{-5} and 4.66×10^{-5} GHz/$\mu\varepsilon$, respectively.

4 Preparation of Panel Specimens

Mix designs of the concrete and mortar used in this study are listed in Table 1. The water-to-cementitious materials' ratio (w/cm) was set to 0.38 by weight. The cementitious materials were composed of Type II Portland cement and Class C fly ash. Both fine and coarse aggregates were used to result in the particle size distribution as shown in Fig. 5 by sieve analysis.[19] The initial setting time of the mortar was determined to be 90 to 120 min by American Society for Testing and Materials standard tests.[20] Super plasticizer was used to improve the flowability of the mixtures.

To protect the optical fibers from damage during construction of the pavement overlay, an installation procedure was developed for the distributed sensors, as illustrated in Fig. 6. In accordance with the actual construction procedure of an unbonded pavement overlay in field application, a 183 cm × 183 cm wood formwork was first built and laid on top of a 3-mm-thick porous fabric sheet. An optical fiber was then deployed and attached with adhesive beads on top of the fabric sheet following a design serpentine pattern, and was finally covered by a thin layer of mortar (5 to 10 mm thick). The adhesive was used to temporarily fix the optical fiber at certain predetermined points and ensure its proper position as designed. The distance between two adjacent points could be 10 to 20 cm. The mortar was dried for about 120 min prior to concrete casting so that it could set and gain some strength.[20] Finally, the concrete pavement panels were cast in a conventional fashion.

With the proposed installation method, all protective optical fibers survived the casting process of three 183 cm × 183 cm × 7.5 cm concrete panels reinforced with alloy polymer macrosynthetic fibers (Fibermesh 650). The three specimens were out of six total panels tested for the overall experimental program and are referred to as P2, P3, and P6. Each panel was instrumented with multiple distributed sensors. The distributed sensors can be deployed in different ways, depending on the specific measurement objectives. For instance, in this study, the sensors were deployed in a serpentine pattern to cover more area in each panel. The diameter of the fibers at all turning areas must be larger than 5 cm. Note that bending a fiber with a small radius

Table 1 Concrete and mortar mixtures (unit: kg/m^3).

Material	Water	Type II Portland cement	Class C fly ash	Natural sand (0-3 mm)	Class C aggregate	Synthetic fibers (40 mm)	Super plasticizer
Concrete	136	250	107	734	1064	3.57	1.78
Mortar	136	250	107	734	N.A.	N.A.	1.78

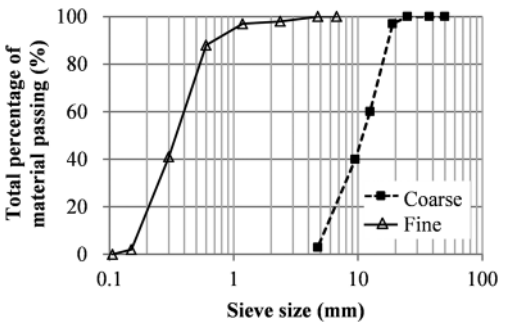

Fig. 5 Distribution of fine and coarse aggregates by sieve analysis.

could result in significant signal loss in the distributed sensor, thus reducing its maximum sensing distance.

5 Experimental Study

5.1 *Experimental Setup*

After 28-day curing, the panels were tested with a three-point bending setup as shown in Fig. 7. The reaction frame with a loading capacity of 445 kN was rigidly fixed on the strong floor and provided two reaction forces through two hydraulic actuators. The two reaction forces were transferred through two orthogonal rigid beams into a line load applied on each panel at its mid-span. Each panel was simply supported on two steel rollers and beams, and loaded in displacement control at a rate of 2 mm/ min. The applied load was recorded by internal load cells in actuators with a 10-Hz sampling frequency. Mid-span deflections and support settlements were measured by linear variable differential transformers. The clear span length between supports was 1.5 m. The Brillouin frequency shifts were measured from the distributed optical fibers using the Neubrescope. Since measurement results from different panels were in good agreement, for simplicity, only the results from Panel P6 are presented and discussed in the following sections. Panel P6 was instrumented with three independent distributed fiber optic sensors (2C #1, 2C #2, and 3C #1), respectively.

5.2 *Experimental Results and Discussion*

5.2.1 *Load-deflection relationship and crack pattern*

Figure 8 shows the mid-span load-deflection relationship of the concrete panel. It can be observed from Fig. 8 that the load was linearly increased until a major crack appeared at 3.6 mm mid-span deflection, then dropped suddenly from 22.3 to 9.7 kN, and was finally increased again with the applied deflection since the microfibers within the concrete matrix and the fabric sheet underneath the panel restrained the crack from widening. However, the slope of the reload-deflection relation is smaller than that prior to the major crack due to softening of the cracked panel. As the panel was further deflected from 20 to 90 mm, the microfibers gradually ruptured or were pulled out of the concrete matrix as observed during tests, resulting in a gradually reduced load of 17.3 to 13.0 kN. Eventually, the panel failed in flexure.

At the completion of tests, the fabric sheet was removed from the tested panel in order to examine the crack pattern in relation to the distributed sensor or optical fiber deployment pattern on the bottom face of the panel. As shown in Fig. 9, capital letters (A to M) marked the turning points of the optical fibers; two major cracks represented by thick dashed lines crossed the optical fibers near mid-span of the panel, and a

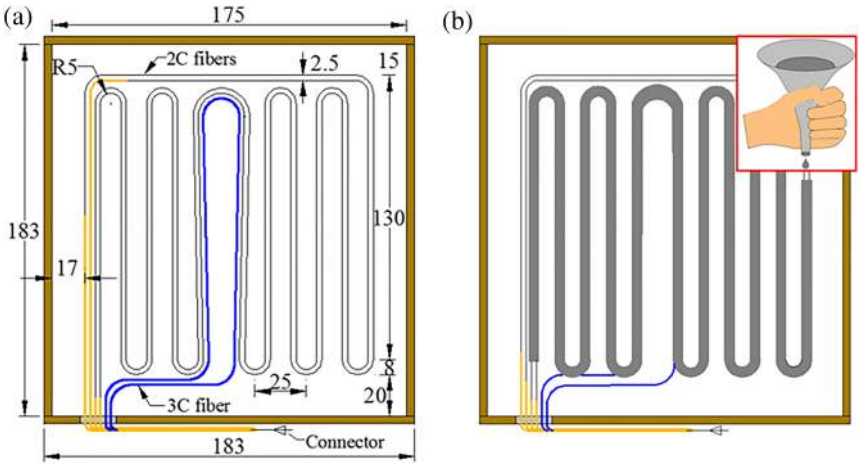

Fig. 6 Sensor installation (unit: cm): (a) fiber layout and (b) mortar casting.

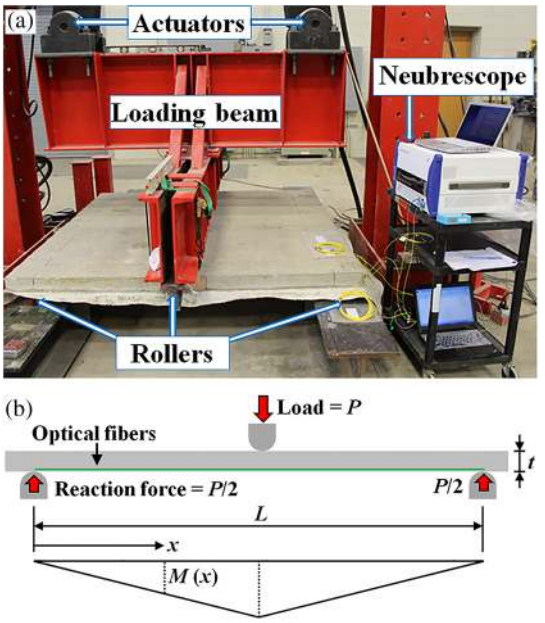

Fig. 7 Three-point bending test: (a) test setup and (b) moment diagram.

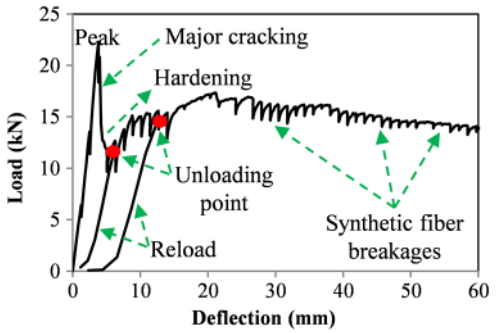

Fig. 8 Mid-span load-deflection relationship.

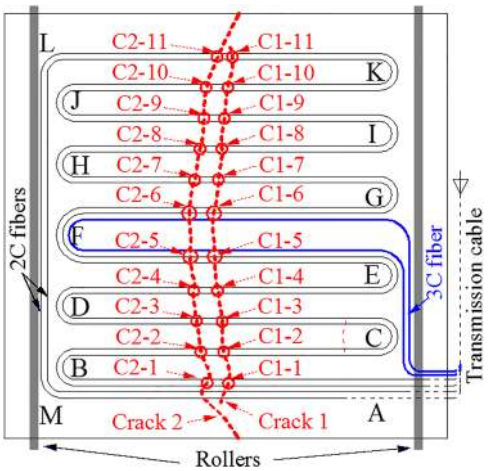

Fig. 9 Crack pattern.

minor crack represented by a thin dashed line occurred near Point "C." The spacing between the two major cracks varied from approximately 8 to 12 cm. The intersection points of the cracks and the optical fibers were designated by "Ca-b," where "C" means a crack, and "a" and "b" represent the number of a crack and the number of the intersection points along the crack. For instance, the first intersection of Crack 1 with the optical fiber was referred to as C1-1.

5.2.2 *Strain distributions prior to cracking*

The tested panel as shown in Fig. 7(a) has a prismatic cross section with uniform material property both longitudinally and transversely. It can be modeled by a simply supported beam as shown in Fig. 7(b) with L span length and t beam height (or panel thickness). The optical fiber is considered to be covered by c depth from the bottom of the beam. Under a concentrated load (P) at mid-span of the beam, the mid-span deflection (d), the bending moment $M(x)$ at cross section x, and the tensile strain $\varepsilon(x)$ at the location of the optical fiber can be expressed as[21]

$$d = PL^3/48EI, \tag{3}$$

$$M(x) = \begin{cases} Px/2, & 0 \le x \le L/2 \\ P(L/2 - x)/2, & L/2 < x \le L \end{cases}, \tag{4}$$

$$\varepsilon(x) = M(x)(t/2 - c)/EI, \tag{5}$$

where EI denotes the flexural stiffness of the cross section. Five 101.6 mm × 203.2 mm (diameter × height) concrete cylinders were tested after 28-day curing. Their average compressive strength was 32.6 MPa, giving an E value of 26.9 GPa according to American Concrete Institute standards.[22] The moment of inertia I was taken as 6.15×10^7 mm^4.

By finding EI from Eq. (3) and substituting the EI and Eq. (4) into Eq. (5), the strain at the fiber location can be written as

$$\varepsilon(x) = \begin{cases} 24d(t/2 - c)x/L^3, & 0 \le x \le L/2 \\ 24d(t/2 - c)(L/2 - x)/L^3, & L/2 < x \le L \end{cases}. \tag{6}$$

Equation (6) indicates that the strain at the location of the optical fiber increases linearly with the mid-span deflection and is linearly distributed over the length of the beam.

During concrete casting, cement paste sunk through approximately 1.5 mm out of the 3-mm-thick porous fabric sheet, thus covering the optical fiber by 1.5 mm from the bottom of the beam. When $L = 1.68$ m, $t = 0.075$ m, and $c = 1.5$ mm, the strain distributions for various mid-span deflections ($d = 1.5$ and 3.0 mm) can be evaluated from Eq. (6) as shown in Fig. 10. At $d = 3.0$ mm, no crack can be visually observed from the test panel or identified from the load-deflection relationship. Therefore, the analytical strain distribution can be directly compared with those measured from the distributed sensors, 2C#1, 2C#2, and 3C#1, as shown in Fig. 10. Since the concrete panel was tested at room temperature inside the Highbay structures laboratory, the measured Brillouin frequency shifts from the distributed sensors can be converted directly into strains based on Eq. (2) with the calibrated strain sensitivity coefficients.

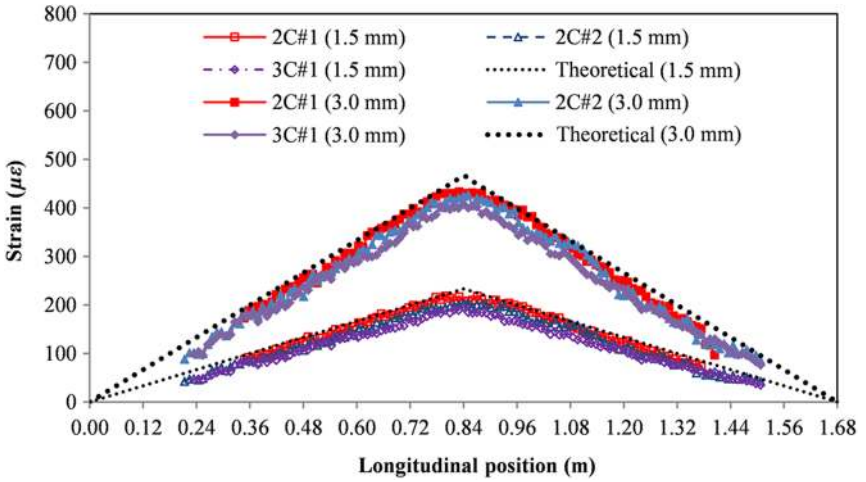

Fig. 10 Strain distributions from theoretical analysis and distributed sensors.

The measured strain distributions in Fig. 10 only cover the part of the panel with deployed optical fibers as shown in Fig. 9.

Overall, the measured strain distributions are in good agreement with the analytical predictions. They differed from the analytical results by 10% to 25%. There are four main reasons for the deviation. First, the strain transfer effect on sensor measurement[23–25] was not taken into account, resulting in underestimated measurements. Second, the point load at mid-span was idealized in analysis. During concrete panel tests, the applied load was actually distributed over a small finite length, which could be notable when compared with the short span of the test panel. As a result, the analytical result at mid-span is likely overestimated. Third, the optical fiber was just placed on top of the 3-mm-thick fabric sheet without control. Due to nonuniformly distributed pressure during concrete casting and a potentially changing concrete mixture over time, the cover depth (c) of the optical fiber may vary over the length of the beam. Finally, the assumption of uniform material property and constant cross section in each panel could induce error. Concrete is a heterogeneous material and its modulus of elasticity is affected by material composition, curing conditions, and loading conditions.[26,27] Thus, the modulus of elasticity could vary in the plane of the test panel. For example, the modulus of concrete in tension could be slightly larger than that in compression.[28]

5.2.3 *Strain distributions after cracking*

Figures 11(a)–11(c) show the measured strain distributions in Panel P6 along the three distributed sensors (2C#1, 2C#2, and 3C#1) corresponding to mid-span deflections of 5 and 6.25 mm. The distance along the optical fiber used in Fig. 11 is measured from the pump end of the Neubrescope. For example, Point "B" was measured at approximately 7.1 m by sensor 2C#1 and 6.8 m by sensor 2C#2. Due to the symmetric behavior of the tested panel and nearly symmetric deployment of the distributed sensor between "I-L" and "E-B," only the measured strains from "A" to "H" are presented in Figs. 11(a) and 11(b) for clarity.

Once a crack initiates and is extended across an optical fiber, the fiber will be locally elongated with significant deformation, thus sensing a sudden increase of strain. Therefore, the crack can be detected and located at a sharp peak of the measured strain distribution from the distributed fiber optic sensor.[29] The identified crack location was found to closely correlate with the physical location of the crack that was determined using a measurement tape.

The magnitude of each strain peak is related to the width of the associated crack. Figures 11(a) and 11(b) indicate that the peak values are different even if they correspond to the same crack. This is because the width of a crack could change in various parts of heterogeneous concrete, and each peak can only represent the local crack width. Additionally, it can be observed that the peak values increase with the loading level, indicating the widening of the associated cracks. Each peak represents the strain over the sensor length at a crack.[23] Due to bonding between the concrete panel and the optical fiber, the optical fiber passing through a crack will be elongated with increased strain as the crack is widening. Furthermore, the propagation of the existing cracks and the appearance of new cracks were detected from the measured strain distributions by the distributed sensors. Two low peaks can be identified near Point "C" as indicated in Fig. 11(b). They represent two microcracks that likely resulted from nonuniform shrinkage in concrete.[9]

To demonstrate the sensor detectability of multiple cracks to the full extent, the spatial resolution for closely spaced cracks is examined. At a mid-span deflection of 5 mm, two cracks C1-2 and C2-2 were observed on the tested panel between Points "B" and "C." Correspondingly, two strain peaks were identified from the strain distribution measured by 2C#1 as shown in Fig. 11(a); however, only one wide peak could be identified from the strain distribution measured by 2C#2 as shown in Fig. 11(b). Although the distributed sensors, 2C#1 and 2C#2, were nearly collocated, both crossing the two cracks, they likely had different spatial resolution for crack detection. Note the difference in spatial resolution for crack detection and strain measurement. Due to potential strain transfer through coating layers of the optical fiber and potential inelastic deformation in the coating materials, the crack-induced sudden change in strain can be redistributed over a length of the optical fiber.[24] If the redistribution length is longer than the spatial resolution for strain measurement, the spatial resolution for crack

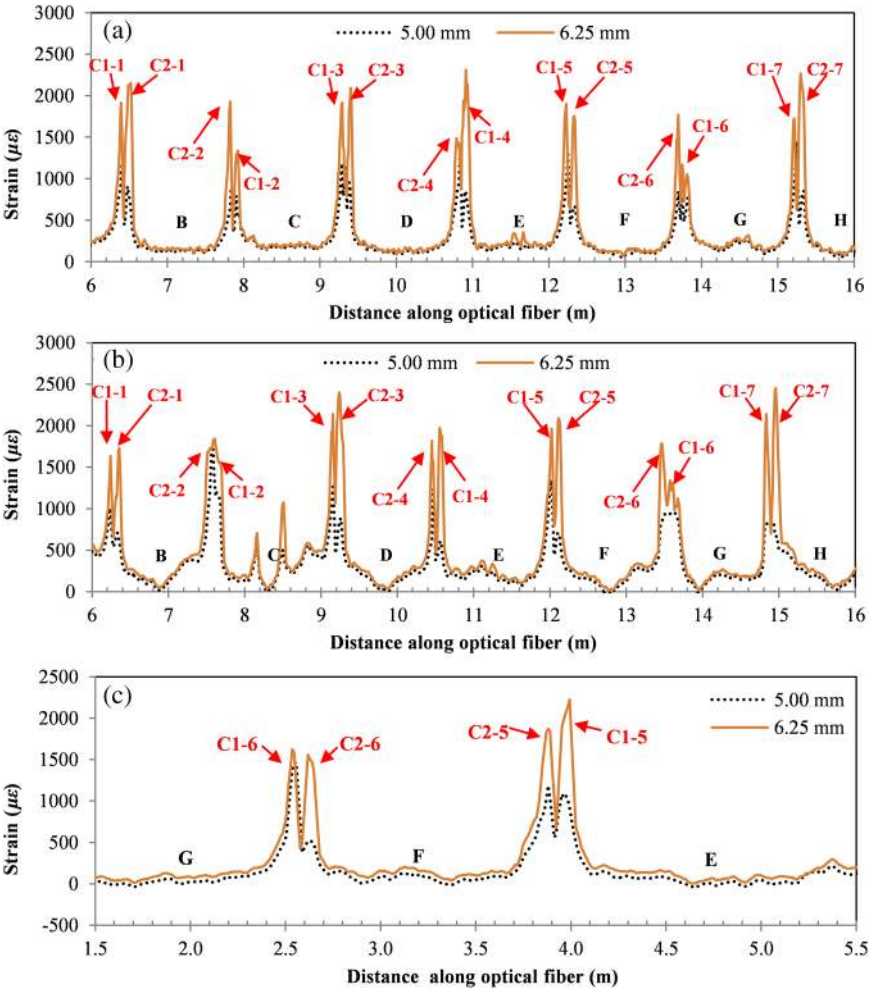

Fig. 11 Strain distributions in P6 measured from: (a) 2C#1, (b) 2C#2, and (c) 3C#1.

detection cannot reach the spatial resolution for strain measurement. However, if the redistribution length is shorter than the spatial resolution for strain measurement, the spatial resolution for crack detection will be the same as the spatial resolution for strain measurement. When debonding between the optical fiber and its coating occurs at a crack,[16] the debonding length will influence the spatial resolution for crack detection as well. Two adjacent cracks are not discernable and are thus considered as one when their spacing is smaller than the spatial resolution for crack detection. In this study, the spacing of two close cracks was measured with a measurement tape. Specifically, cracks C1-2 and C2-2 were approximately 9 and 7 cm apart when they crossed sensors 2C#1 and 2C#2, respectively. The spacing of the two cracks at other locations ranged from 9 to 12 cm. Once crossed by the sensors elsewhere, the two cracks could be clearly identified from the measured strain distributions as shown in Fig. 11. Therefore, the spatial resolution for crack detection is approximately 7 to 9 cm. Further studies are needed for a more precise determination of the spatial resolution for crack detection.

6 Conclusions

In this study, a distributed fiber optic sensing technology based on PPP-BOTDA has been successfully implemented for the first time to measure strain distribution and detect multiple cracks in thin concrete pavement panels. To protect them from damage during installation, optical fibers can be covered with 5 to 10 mm of mortar that is set for 2 h prior to concrete casting.

As distributed sensors, single-mode optical fibers packaged with two and three layers of coating can sustain a maximum strain of approximately 2.33% and 2.42%, respectively. Their strain sensitivity coefficients are 5.43×10^{-5} and 4.66×10^{-5} GHz/$\mu\varepsilon$, respectively. With the calibrated sensitivity coefficient, the directly measured Brillouin frequency shift was converted into strain distribution. The measured strain distribution from the distributed sensor was in general agreement with the analytical prediction. Their difference is 10% to 25%, which is mainly due to the strain transfer effect in coated optical fiber, idealized point load in analysis, varying sensor embedment, and concrete heterogeneity.

Multiple cracks in concrete panels were detected and located at sharp strain peaks of the measured strain distributions. The spatial resolution of crack detection was demonstrated to be at least 7 to 9 cm. The widening and propagation of cracks were detected. The two-layer coated fiber is more sensitive to cracking than the three-layer coated fiber.

Acknowledgments

This study was partially supported by the U.S. Department of Transportation under Grant No. DTRT06-G-0014-NUTC,

and by Mid-America Transportation Center under Grant No. 25-1121-0003-196. Authors would like to express their deep appreciation to two anonymous reviewers for their constructive comments and suggestions.

References

1. D. Harrington and G. Fick, "Guide to concrete overlays: sustainable solutions for resurfacing and rehabilitating existing pavements," Technical Report ACPA Publication TB021.03P, National Concrete Pavement Technology Center, Washington, DC (2014).
2. A. M. Ioannides and S. Sengupta, "Crack propagation in Portland cement concrete beams: implications for pavement design," *J. Transp. Res. Board* **1853**, 110–117 (2003).
3. M. Liao, "Towards fracture mechanics-based design of unbonded concrete overlay pavements," PhD Thesis, Univ. of Minnesota (2011).
4. Z. Zhou et al., "Optical fiber Bragg grating sensor assembly for 3D strain monitoring and its case study in highway pavement," *Mech. Syst. Signal Process.* **28**, 36–49 (2012).
5. Y. Zhao and F. Ansari, "Quasi-distributed fiber-optic strain sensor: principle and experiment," *Appl. Opt.* **40**(19), 3176–3181 (2001).
6. M. Azenha, R. Faria, and D. Ferreira, "Identification of early-age concrete temperatures and strains: monitoring and numerical simulation," *Cem. Concr. Compos.* **31**, 369–78 (2009).
7. C. Ouyang, E. Landis, and S. Shah, "Damage assessment in concrete using quantitative acoustic emission," *J. Eng. Mech.* **117**(11), 2681–2698 (1991).
8. G. Chen et al., "Crack detection of a full-scale reinforced concrete girder with a distributed cable sensor," *Smart Mater. Struct.* **14**(3), S88–S97 (2005).
9. Y. Bao et al., "Measuring mortar shrinkage and cracking by pulse pre-pump Brillouin optical time domain analysis with a single optical fiber," *Mater. Lett.* **145**, 344–346 (2015).
10. X. Bao and L. Chen, "Recent progress in Brillouin scattering based fiber sensors," *Sensors* **11**, 4152–4187 (2011).
11. X. Bao and L. Chen, "Recent progress in distributed fiber optic sensors," *Sensors* **12**, 8601–8639 (2012).
12. A. Mufti et al., "Crack detection of steel girders using Brillouin optical time domain analysis," *J. Civ. Struct. Health Monit.* **1**(3-4), 61–68 (2011).
13. J. Gao et al., "Monitoring the stress of the post-tensioning cable using fiber optic distributed strain sensor," *Measurement* **39**, 420–428 (2006).
14. M. H. Motamedi et al., "Quantitative investigation in distributed sensing of structural defects with Brillouin optical time domain reflectometry," *J. Intell. Mater. Syst. Struct.* **24**(10), 1187–1196 (2013).
15. N. A. Hoult, O. Ekim, and R. Regier, "Damage/deterioration detection for steel structures using distributed fiber optic strain sensors," *J. Eng. Mech.* **140**(12), 04014097 (2014).
16. B. Glisic and D. Inaudi, "Development of method for in-service crack detection based on distributed fiber optic sensors," *Struct. Health Monit.* **11**(2), 161–171 (2011).
17. K. Kishida and C. H. Li, "Pulse pre-pump-BOTDA technology for new generation of distributed strain measuring system," in *Proc. Structural Health Monitoring and Intelligent Infrastructure*, pp. 471–477, London, UK, (2006).
18. G. Chen et al., "Pilot study on rugged fiber optic Brillouin sensors for large-strain measurements to ensure the safety of transportation structures," Technical Report MATC-25-1121-0001-114 and MATC-25-1121-0001-242, (Mid-America Transportation Center 2012).
19. ASTM C136/C136M–14, "Standard test method for sieve analysis of fine and coarse aggregates," American Society for Testing and Materials, Pennsylvania, USA (2014).
20. ASTM C403/C403M–08, "Standard test method for time of setting of concrete mixtures by penetration resistance," American Society for Testing and Materials, Pennsylvania, USA (2008).
21. J. M. Gere, Ed., *Mechanics of Materials*, 6th ed., Thomson Learning, Belmont, California (2004).
22. ACI 318-14, "Building code requirements for structural concrete and commentary," American Concrete Institute, USA (2014).
23. D. Li et al., "Strain transferring analysis of fiber Bragg grating sensors," *Opt. Eng.* **45**(2), 024402 (2006).
24. F. Ansari and Y. Libo, "Mechanics of bond and interface shear transfer in optical fiber sensors," *J. Eng. Mech.* **124**(4), 385–394 (1998).
25. X. Feng et al., "Theoretical and experimental investigations into crack detection with BOTDR-distributed fiber optic sensors," *J. Eng. Mech.* **139**, 1797–1807 (2013).
26. T. Noguchi et al., "A practical equation for elastic modulus of concrete," *ACI Struct. J.* **106**(5), 690–696 (2009).
27. H. Wang and Q. Li, "Prediction of elastic modulus and Poisson's ratio for unsaturated concrete," *Int. J. Solids Struct.* **44**(5), 1370–1379 (2007).
28. I. Yoshitake et al., "A prediction method of tensile young's modulus of concrete at early age," *Adv. Civ. Eng.* **2012**, 391214 (2012).
29. A. Deif et al., "Detection of cracks in a reinforced concrete beam using distributed Brillouin fibre sensors," *Smart Mater. Struct.* **19**(5), 055014 (2010).

Yi Bao received his BS and MS degrees in civil engineering from Southwest Jiaotong University (China) in 2009 and 2011, respectively. Currently, he is a PhD candidate in civil engineering at Missouri University of Science and Technology (formerly University of Missouri, Rolla), USA. His research interests include concrete pavements, nondestructive evaluation, structural health monitoring, and distributed fiber optic sensors.

Genda Chen received his PhD from the State University of New York at Buffalo in 1992 and joined Missouri University of Science and Technology in 1996 after three years of bridge engineering practice. He is a professor and Abbett Distinguished Chair in civil engineering. He authored over 300 publications in structural health monitoring, structural control, interface mechanics and deterioration, and earthquake engineering. He is a fellow of ASCE and SEI.